LETTER

Stellar Bars in Isolated Gas-Rich Spiral Galaxies Do Not Slow Down

Angus Beane[1*], Lars Hernquist[1], Elena D'Onghia[2,3], et al.

Elongated bar-like features are ubiquitous, occurring at the centers of approximately two-thirds of spiral disk galaxies [1,2]. Due to gravitational interactions between the bar and the other components of galaxies, it is expected that angular momentum and matter will redistribute between galactic components over long (Gyr) timescales in galaxies hosting a bar [3–5]. Previous work has overwhelmingly provided the expectation that, due to the interaction between the bar and the dark matter halo, the bar pattern will slow its rotation over time [6–15]. We have performed a simulation of a Milky Way-like galactic disk hosting a strong bar which includes a state-of-the-art model of the interstellar medium and a live dark matter halo. In this simulation the bar pattern does not slow down over time, and instead remains at a stable, constant rate of rotation. This behavior has been observed in previous simulations but its explanation has remained elusive.[16,17]. We propose that the gas phase of the disk and the dark matter halo act in concert to stabilize the bar pattern and prevent it from slowing down or speeding up. This result naturally explains why nearly all observed bars rotate quickly[18–20] and is especially relevant for our understanding of how the Milky Way arrived at its present day state.

It has long been known that non-axisymmetric features in a stellar disk act to redistribute mass and angular momentum.[3] The interaction between a bar and a spheroid (either a dark matter halo or stellar bulge) has received considerable interest.[4,5] A stellar disk in isolation seems to always generate a bar instability,[21] but the presence of a strong spherical potential (e.g., from a stellar bulge or dark matter halo) acts to stabilize the disk against the bar instability.[22,23] A number of numerical simulations have confirmed that a live dark matter halo generically exerts a negative torque on the bar, causing its pattern speed to decrease and its length and strength to increase[6–15]. Intuitively, the bar excites a wake of resonant material in the dark matter halo in a manner similar to dynamical friction. This wake lags and thus exerts a negative torque on the bar.

The preeminent expectation that the dark matter halo acts to slow the bar down conflicts with observational estimates of bar pattern speeds. Bar rotation rates are typically classified by the dimensionless ratio

$$\mathcal{R} = R_{\rm CR}/R_b, \tag{1}$$

where $R_{\rm CR}$ is the radius of corotation and R_b is the length of the bar. Galaxies with $\mathcal{R} < 1.4$ are considered "fast rotators" while galaxies with $\mathcal{R} > 1.4$ are considered "slow rotators."[7] Galaxies with $\mathcal{R} < 1$ are not thought to be stable.[24] Observational estimates of the pattern speeds of bars indicate that nearly all galaxies have $1 < \mathcal{R} < 1.4$.[18–20]

The role of gas on the evolution of the bar is less well-understood. Since the gas phase typically only contributes about $10 - 20\%$ of the mass of a galaxy at the present day, one might naively expect it to have a subdominant effect on the bar. However, because gas is collisional, it can participate in non-resonant angular momentum exchange with the bar.[25] Thus, numerical work has shown that the gas phase has an outsized influence on the bar.[17,26]

We have performed a simulation of a disk galaxy using the finite-volume gravito-hydrodynamics code AREPO.[27] In AREPO, the fluid is discretized as a moving Voronoi mesh. We use the additional physics in the galaxy formation module Stars and MUltiphase Gas in GaLaxiEs (SMUGGLE) [28]. SMUGGLE is a comprehensive and self-consistent galaxy formation model with a wide range of physical processes, including radiative heating/cooling, star formation, and stellar feedback. More detailed information on SMUGGLE is given in the Methods section. Our disk galaxy is a modified version of the GALAKOS model[29], which consists of a stellar disk, stellar bulge, and dark matter halo. After $\sim 2.5\,$Gyr of evolution, the GALAKOS disk forms a bar consistent with the Milky Way bar in terms of pattern speed and length ($\sim 40\,$km/s/kpc and $\sim 4.5\,$kpc, respectively). We modify this setup to include a gas phase, the details of which is given in the Methods section.

A surface density projection of our simulations is shown in Fig. 1. The upper three panels show the disk in the N-body run while the lower three panels show the disk in the SMUGGLE run. Each column shows the disk $\sim 1\,$Gyr apart in time. There is a large qualitative difference in the evolution of the bar pattern between the two runs. We see that in the N-body case, the bar lengthens in time and grows in strength. In the SMUGGLE case, the bar pattern retains a similar length and strength between panels.

We show the time evolution of different bar properties in Fig. 2. In the upper panel, we show the pattern speed over time in the N-body (blue) and SMUGGLE (orange) runs. The pattern speed in the N-body case slows down while the pattern speed in the SMUGGLE case remains constant. The slowing down of the pattern speed in the N-body case is consistent with a long line of numerical research on bars in N-body simulations.[6–15] How-

[1]Center for Astrophysics | Harvard & Smithsonian, Cambridge, MA, USA
[2]Department of Physics, University of Wisconsin-Madison, Madison, WI, USA
[3]Department of Astronomy, University of Wisconsin-Madison, Madison, WI, USA
* angus.beane@cfa.harvard.edu

The radius of corotation $R_{\rm CR}$ is defined for circular orbits as the radius at which the orbital frequency is equal to the pattern speed, Ω_p, of a given non-axisymmetric feature. In a galaxy with a constant circular velocity V_c, it is given by $R_{\rm CR} = V_c/\Omega_p$.

ever, in the SMUGGLE case the pattern speed remains constant. After the first Gyr of evolution, we find that the pattern speed increases by only $\sim 10\%$ over the next 4 Gyr, compared to a $\sim 43\%$ decrease in the pattern speed for the N-body run over the same interval. As we saw qualitatively in Fig. 1, the length of the bar in the N-body case grows over time while it remains constant in the SMUGGLE case. This is also consistent with previous numerical work, which found that bars tend to grow as they slow down and the radius of corotation increases.[7,10]

The bottom panel of Fig. 2 shows the torque exerted on the bar by different components. The solid lines indicate the torque on the bar by the dark matter halo whereas the dashed line indicates the torque on the bar by the gas phase. In the N-body case, the halo exerts a steady negative torque on the bar, with an average torque from 1 to 4 Gyr of -58.0 in units of $10^{10} M_{\odot}$ (km/s)^2. The halo in the SMUGGLE case exerts a similar negative torque on the bar in the first Gyr of evolution, but after that the halo exerts a much smaller torque on the bar, averaging only -7.8 in the same units and over the same interval. The gas in the SMUGGLE case exerts a steady positive torque averaging 11.7 in the same units and over the same interval.

The fact that the dark matter halo in the SMUGGLE case exerts a smaller positive torque on the bar can be understood in terms of the halo wake mechanism. In the N-body case, halo material which is resonant with the bar will form a wake which lags behind and exerts a negative torque on the bar, which slows it down.[4–6] As the bar slows down, the location of the resonances in phase space changes, allowing halo material newly resonant with the bar to form a new wake. However, the gas is a reliable source of positive torque on the bar, speeding the bar up. This stops the resonance location from changing such that the halo cannot form a new wake, arresting the process by which the halo can slow the bar down.

We can test this interpretation by measuring the angle offset between the halo wake and the bar. If the wake and the bar are aligned (i.e., there is no angle offset), then the wake cannot exert a negative torque on the bar. This angle is plotted in the middle panel of Fig. 3, which shows that the angle offset is larger in the N-body case than in the SMUGGLE case by about a factor of two. The left and right panels of Fig. 3 show the halo wake with respect to the location of the bar in the N-body (left) and SMUGGLE (right) cases.

The presence of the gas can arrest the process by which the dark matter halo wake forms. However, this does not explain why the pattern speed in the SMUGGLE case is nearly constant over several Gyr. Naively, it would be a coincidence that the bar pattern speed remains constant in the SMUGGLE case, resulting from a chance cancellation of the halo and gas torques. However, a constant pattern speed in the presence of gas has been observed in a few simulations of barred galaxies with gas.[16,17] Previous work has argued this is due to the bar torquing gas inwards, but no explanation has been given for why it might remain constant.

We propose that an equilibrium mechanism is responsible for the pattern speed remaining approximately constant. In this scenario, a torque must oppose changes in the pattern speed so that when the bar speeds up, a negative torque will slow it down and when the bar slows down, a positive torque will speed it up. It is simple to explain the first of these - when the pattern speed increases, the location of resonances will shift to regions of the dark matter halo phase space where no wake has been excited yet (e.g., the corotation radius will shrink).

When the bar slows down, we argue that this induces a larger positive torque from the gas phase. Only gas within corotation will flow inwards, while gas outside corotation will flow outwards.[25] Since the corotation radius is larger for more slowly rotating bars, it follows that more slowly rotating bars should be more efficient at driving gas inflows and thus experience a larger positive torque from the gas phase.

We performed an experiment to test this hypothesis by forcing the stellar disk in the SMUGGLE run to rotate at a constant angular rate and measuring the torque on the bar by the gas phase at different rotation rates. The result of this experiment is shown in Fig. 4, which shows that a more slowly rotating bar experiences a larger positive torque from the gas. We have therefore shown evidence for an equilibrium mechanism which keeps the pattern speed of the bar constant, resulting from the complex interplay between the dark matter halo and the gas phase.

The implications of this finding are numerous. First, we naturally explain why nearly all observed galaxies are fast rotators without requiring the inner regions of dark matter halos to be underdense[7,30] or introducing new physics.[31,32] Second, we show that the role of gas is of paramount importance in studies which attempt to uncover the nature of dark matter from its effect of slowing down the bar.[33,34] Third, we provide an explanation for how the Milky Way's bar could be both long-lived and a fast rotator, of which there is some observational evidence.[35] And finally, we complicate the picture of radial mixing expected to sculpt the Milky Way's disk [36,37], a process which relies upon the pattern speed of the bar to change with time (though our work does not alter expectations for radial mixing induced by spiral arms[38]).

Barred galaxies in cosmological simulations of galaxy formation continue to be in conflict with observations by producing bars which rotate too slowly.[39–41] However, the pattern speeds of bars in both cosmological simulations and the real universe can be affected by environmental processes not included in our simulation – e.g., satellite infall[42], non-sphericity[26] or rotation[43–46] in the dark matter halo, or perhaps even the gaseous circumgalactic medium. Naturally, extending our present work to account for such effects is a crucial next step in understanding the formation and evolution of galactic bars.

Since the bar is not a solid body, it is not guaranteed that a negative torque will slow it down - e.g. a negative torque could shred the bar, reducing its moment of inertia without changing its pattern speed. However, the bar seems to empirically respond to a negative torque induced by a halo wake by slowing down.

1. Eskridge, P. B. *et al.* The Frequency of Barred Spiral Galaxies in the Near-Infrared. AJ **119**, 536–544 (2000). astro-ph/9910479.
2. Menéndez-Delmestre, K., Sheth, K., Schinnerer, E., Jarrett, T. H. & Scoville, N. Z. A Near-Infrared Study of 2MASS Bars in Local Galaxies: An Anchor for High-Redshift Studies. ApJ **657**, 790–804 (2007). astro-ph/0611540.
3. Lynden-Bell, D. & Kalnajs, A. J. On the generating mechanism of spiral structure. MNRAS **157**, 1 (1972).
4. Tremaine, S. & Weinberg, M. D. Dynamical friction in spherical systems. MNRAS **209**, 729–757 (1984).
5. Weinberg, M. D. Evolution of barred galaxies by dynamical friction. MNRAS **213**, 451–471 (1985).
6. Hernquist, L. & Weinberg, M. D. Bar-Spheroid Interaction in Galaxies. ApJ **400**, 80 (1992).
7. Debattista, V. P. & Sellwood, J. A. Constraints from Dynamical Friction on the Dark Matter Content of Barred Galaxies. ApJ **543**, 704–721 (2000). astro-ph/0006275.
8. Athanassoula, E. & Misiriotis, A. Morphology, photometry and kinematics of N -body bars - I. Three models with different halo central concentrations. MNRAS **330**, 35–52 (2002). astro-ph/0111449.
9. Athanassoula, E. Bar-Halo Interaction and Bar Growth. ApJ **569**, L83–L86 (2002). astro-ph/0203368.
10. Athanassoula, E. What determines the strength and the slowdown rate of bars? MNRAS **341**, 1179–1198 (2003). astro-ph/0302519.

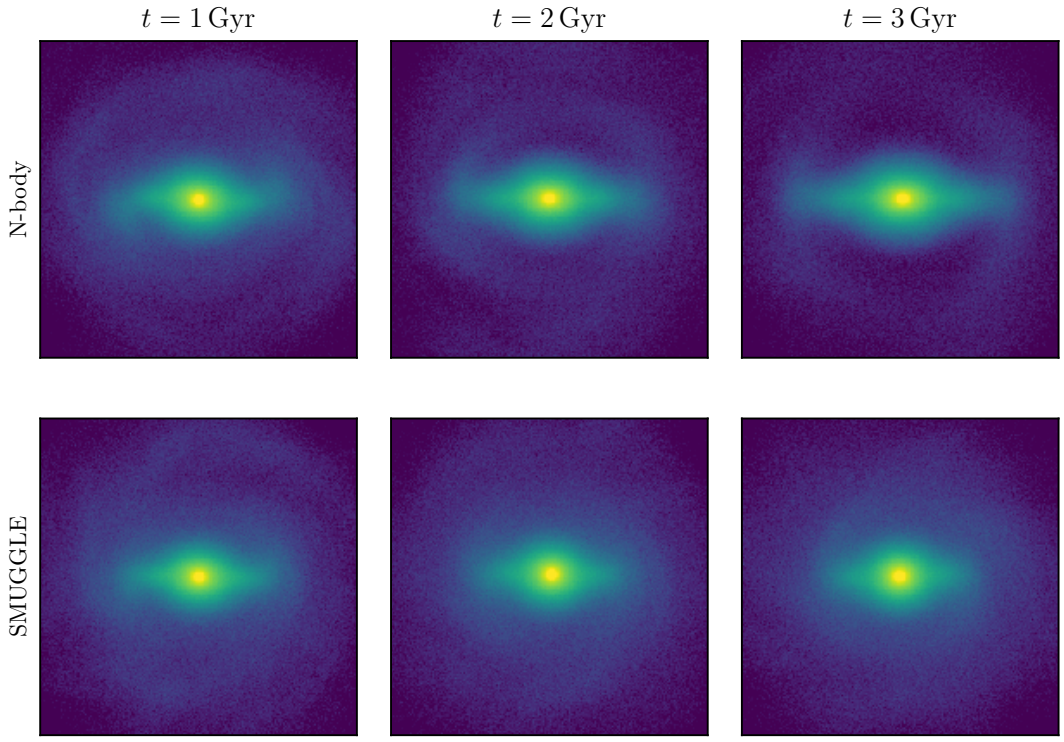

Figure 1: Surface density projections in an N-body only simulation (upper panels) and a simulation which includes the SMUGGLE model (bottom panels). We can see that in the N-body run, the bar grows in length and strength. In the SMUGGLE run (which includes a gaseous phase and a model for the multi-phase interstellar medium), the bar remains at approximately the same length and strength over the course of the simulation. The N-body model is identical to the GALAKOS model, discussed in the text.

11. O'Neill, J. K. & Dubinski, J. Detailed comparison of the structures and kinematics of simulated and observed barred galaxies. MNRAS **346**, 251–264 (2003). astro-ph/0305169.
12. Holley-Bockelmann, K., Weinberg, M. & Katz, N. Bar-induced evolution of dark matter cusps. MNRAS **363**, 991–1007 (2005). astro-ph/0306374.
13. Martinez-Valpuesta, I., Shlosman, I. & Heller, C. Evolution of Stellar Bars in Live Axisymmetric Halos: Recurrent Buckling and Secular Growth. ApJ **637**, 214–226 (2006). astro-ph/0507219.
14. Weinberg, M. D. & Katz, N. The bar-halo interaction - II. Secular evolution and the religion of N-body simulations. MNRAS **375**, 460–476 (2007). astro-ph/0601138.
15. Dubinski, J., Berentzen, I. & Shlosman, I. Anatomy of the Bar Instability in Cuspy Dark Matter Halos. ApJ **697**, 293–310 (2009). 0810.4925.
16. Friedli, D. & Benz, W. Secular evolution of isolated barred galaxies. I. Gravitational coupling between stellar bars and interstellar medium. A&A **268**, 65–85 (1993).
17. Villa-Vargas, J., Shlosman, I. & Heller, C. Dark Matter Halos and Evolution of Bars in Disk Galaxies: Varying Gas Fraction and Gas Spatial Resolution. ApJ **719**, 1470–1480 (2010). 1004.4899.
18. Corsini, E. M. Direct measurements of bar pattern speeds. *Memorie della Societa Astronomica Italiana Supplementi* **18**, 23 (2011). 1002.1245.
19. Aguerri, J. A. L. *et al.* Bar pattern speeds in CALIFA galaxies. I. Fast bars across the Hubble sequence. A&A **576**, A102 (2015). 1501.05498.
20. Guo, R. *et al.* SDSS-IV MaNGA: pattern speeds of barred galaxies. MNRAS **482**, 1733–1756 (2019). 1810.03257.
21. Hohl, F. Numerical Experiments with a Disk of Stars. ApJ **168**, 343 (1971).
22. Ostriker, J. P. & Peebles, P. J. E. A Numerical Study of the Stability of Flattened Galaxies: or, can Cold Galaxies Survive? ApJ **186**, 467–480 (1973).
23. Hohl, F. Suppression of bar instability by a massive halo. AJ **81**, 30–36 (1976).
24. Contopoulos, G. How far do bars extend. A&A **81**, 198–209 (1980).
25. Hopkins, P. F. & Quataert, E. An analytic model of angular momentum transport by gravitational torques: from galaxies to massive black holes. MNRAS **415**, 1027–1050 (2011). 1007.2647.
26. Athanassoula, E., Machado, R. E. G. & Rodionov, S. A. Bar formation and evolution in disc galaxies with gas and a triaxial halo: morphology, bar strength and halo properties. MNRAS **429**, 1949–1969 (2013). 1211.6754.
27. Springel, V. E pur si muove: Galilean-invariant cosmological hydrodynamical simulations on a moving mesh. MNRAS **401**, 791–851 (2010). 0901.4107.
28. Marinacci, F., Sales, L. V., Vogelsberger, M., Torrey, P. & Springel, V. Simulating the interstellar medium and stellar feedback on a moving mesh: implementation and isolated galaxies. MNRAS **489**, 4233–4260 (2019). 1905.08806.
29. D'Onghia, E. & L. Aguerri, J. A. Trojans in the Solar Neighborhood. ApJ **890**, 117 (2020). 1907.08484.
30. Debattista, V. P. & Sellwood, J. A. Dynamical Friction and the Distribution of Dark Matter in Barred Galaxies. ApJ **493**, L5–L8 (1998). astro-ph/9710039.
31. Roshan, M. *et al.* Barred spiral galaxies in modified gravity theories. MNRAS **503**, 2833–2860 (2021). 2103.01794.
32. Roshan, M. *et al.* Fast galaxy bars continue to challenge standard cosmology. MNRAS **508**, 926–939 (2021). 2106.10304.
33. Chiba, R., Friske, J. K. S. & Schönrich, R. Resonance sweeping by a decelerating Galactic bar. MNRAS **500**, 4710–4729 (2021). 1912.04304.
34. Chiba, R. & Schönrich, R. Tree-ring structure of Galactic bar resonance. MNRAS **505**, 2412–2426 (2021). 2102.08388.
35. Bovy, J. *et al.* Life in the fast lane: a direct view of the dynamics, formation, and evolution of the Milky Way's bar. MNRAS **490**, 4740–4747 (2019). 1905.11404.
36. Bird, J. C., Kazantzidis, S. & Weinberg, D. H. Radial mixing in galactic discs: the effects of disc structure and satellite bombardment. MNRAS **420**, 913–925 (2012). 1104.0933.

37. Hayden, M. R. *et al.* Chemical Cartography with APOGEE: Metallicity Distribution Functions and the Chemical Structure of the Milky Way Disk. ApJ **808**, 132 (2015). 1503.02110.
38. Sellwood, J. A. & Binney, J. J. Radial mixing in galactic discs. MNRAS **336**, 785–796 (2002). astro-ph/0203510.
39. Algorry, D. G. *et al.* Barred galaxies in the EAGLE cosmological hydrodynamical simulation. MNRAS **469**, 1054–1064 (2017). 1609.05909.
40. Peschken, N. & Łokas, E. L. Tidally induced bars in Illustris galaxies. MNRAS **483**, 2721–2735 (2019). 1804.06241.
41. Fragkoudi, F. *et al.* Revisiting the tension between fast bars and the ΛCDM paradigm. A&A **650**, L16 (2021). 2011.13942.
42. Purcell, C. W., Bullock, J. S., Tollerud, E. J., Rocha, M. & Chakrabarti, S. The Sagittarius impact as an architect of spirality and outer rings in the Milky Way. Nature **477**, 301–303 (2011). 1109.2918.
43. Saha, K. & Naab, T. Spinning dark matter haloes promote bar formation. MNRAS **434**, 1287–1299 (2013). 1304.1667.
44. Long, S., Shlosman, I. & Heller, C. Secular Damping of Stellar Bars in Spinning Dark Matter Halos. ApJ **783**, L18 (2014). 1402.1491.
45. Collier, A., Shlosman, I. & Heller, C. What makes the family of barred disc galaxies so rich: damping stellar bars in spinning haloes. MNRAS **476**, 1331–1344 (2018). 1712.02802.
46. Collier, A., Shlosman, I. & Heller, C. Dark matter bars in spinning haloes. MNRAS **488**, 5788–5801 (2019). 1811.00033.
47. Springel, V. & Hernquist, L. Cosmological smoothed particle hydrodynamics simulations: a hybrid multiphase model for star formation. MNRAS **339**, 289–311 (2003). astro-ph/0206393.
48. Hopkins, P. F. *et al.* FIRE-2 simulations: physics versus numerics in galaxy formation. MNRAS **480**, 800–863 (2018). 1702.06148.
49. Springel, V., Di Matteo, T. & Hernquist, L. Modelling feedback from stars and black holes in galaxy mergers. MNRAS **361**, 776–794 (2005). astro-ph/0411108.
50. Hernquist, L. An Analytical Model for Spherical Galaxies and Bulges. ApJ **356**, 359 (1990).
51. Vasiliev, E. AGAMA: action-based galaxy modelling architecture. MNRAS **482**, 1525–1544 (2019). 1802.08239.
52. Eilers, A.-C., Hogg, D. W., Rix, H.-W. & Ness, M. K. The Circular Velocity Curve of the Milky Way from 5 to 25 kpc. ApJ **871**, 120 (2019). 1810.09466.
53. Kennicutt, R. C. & Evans, N. J. Star Formation in the Milky Way and Nearby Galaxies. ARA&A **50**, 531–608 (2012). 1204.3552.
54. Grand, R. J. J. *et al.* The Auriga Project: the properties and formation mechanisms of disc galaxies across cosmic time. MNRAS **467**, 179–207 (2017). 1610.01159.
55. Petersen, M. S., Weinberg, M. D. & Katz, N. Dark matter trapping by stellar bars: the shadow bar. MNRAS **463**, 1952–1967 (2016). 1602.04826.
56. Hernquist, L. & Katz, N. TREESPH: A Unification of SPH with the Hierarchical Tree Method. ApJS **70**, 419 (1989).

Acknowledgements Foo.

Author Contributions Foo.

Data Availability Foo.

Code Availability Foo.

METHODS

SMUGGLE Model

We use the Stars and MUltiphase Gas in GaLaxiEs (SMUGGLE) model [28] implemented within the moving-mesh, finite-volume hydrodynamics code AREPO [27]. The SMUGGLE model includes self-gravity, hydrodynamics, radiative heating and cooling, star formation, and stellar feedback. Explicit gas cooling and heating of the multi-phase interstellar medium is implemented, covering temperature ranges between 10 and 10^8 K.

Star formation occurs in cells above a density threshold ($n_{\rm th} = 100\,{\rm cm}^{-3}$) according to ref.[47] with a star-formation efficiency of $\epsilon = 0.01$. Star formation converts gas cells into star particles which represent single stellar populations. For each star particle, the deposition of energy, momentum, and mass from stellar winds and supernovae is modeled. Photo-ionization and radiation pressure are modeled using an approximate treatment. A more detailed description of this model can be found in the flagship SMUGGLE paper.[28]

We used the fiducial model parameters, except that we increased the number of effective neighbors $N_{\rm ngb}$ for the deposition of feedback from 64 to 512. We found that a lower value of $N_{\rm ngb}$ resulted in inefficient photo-ionization feedback since the photo-ionizing budget had not been exhausted after deposition into 64 neighboring cells. We also used an updated version of SMUGGLE using a new mechanical feedback routine similar to the one described in ref.[48] This updated routine is a tensor renormalization which ensures linear and angular momentum conservation to machine precision.

Wind Model

In addition to the SMUGGLE model, we considered a simpler model of the interstellar medium based upon

Initial Setup

The initial setup of the galactic disk used in this work follows closely the GALAKOS model[29], which uses a modified version of `MakeNewDisk`.[49] The GALAKOS model has three components - a radially exponential and vertically isothermal stellar disk, and a stellar bulge and dark matter halo following a Hernquist profile.[50] All N-body runs in this work used the same setup parameters as the GALAKOS disk, more details of which can be found in the original paper.

The addition of the gas phase was done as follows. The version of `MakeNewDisk` used for the original GALAKOS model can generate a gas disk which is radially exponential and in vertical gravito-hydrodynamic balance. We modified the radial profile of this code in order to allow us to generate a disk with a constant surface density within some cut-off radius, and then exponentially declining beyond that radius with the scale-length of the stellar disk. We used an initial surface density of $20\,M_\odot/{\rm pc}^2$ and a cut-off radius of $9.3\,{\rm kpc}$.

After generating the gaseous disk in this way, we stitched the gas disk together with the GALAKOS N-body disk (and bulge and dark matter halo) after the GALAKOS disk has been allowed to evolve for $1.5\,{\rm Gyr}$. The purpose of allowing the GALAKOS disk to evolve first for a short period of time is to allow for the bar to form unimpacted by the presence of the gas (which would normally disrupt the formation of the bar). Throughout this work, we consider $t = 0$ for the N-body run to be the time at which we added the gas phase for the SMUGGLE run (i.e. we ignore the first $1.5\,{\rm Gyr}$ of evolution of the N-body disk when the bar is

forming). We made one additional modification when stitching the gas disk together with the N-body disk - we created a vacuum within the central 4 kpc. This vacuum guards against an initial dramatic infall of gas within the bar region, which we found to destroy the bar.

Our setup is initially out of equilibrium, but we found that after ~ 500 Myr, the entire system has settled into a steady-state configuration and initial transients appear not to affect the results after this point. The constant surface density of the initial gas disk is important for ensuring the gas disk is dense enough in order for comparisons to real galaxies to be appropriate.

We computed the circular velocity curve of our model using the `AGAMA` package.[51] We fit the baryonic component (stellar disk, bulge, gas, and newly formed stars) with an axisymmetric cylindrical spline with 20 grid points in both the radial and vertical direction spanning 0.2 to 50 kpc in the radial direction and from 0.02 to 10 kpc in the vertical direction. We fit the dark matter halo using a spherically symmetric multipole fit with a maximum angular harmonic coefficient of $l = 2$. We plot the circular velocity curve in Extended Data Fig. 1 compared to observational estimates.[52] Our disk is slightly more massive than the Milky Way disk, and in the SMUGGLE run the addition of the gas phase results in a slightly higher circular velocity. We also show the evolution of the surface density profile in Extended Data Fig. 2 compared to observational estimates.[53]

We used a mass resolution of $7.5 \times 10^3\, M_\odot$ for the baryonic components (initial stellar disk, stellar bulge, and gas) and a mass resolution of $3.75 \times 10^4\, M_\odot$ for the dark matter halo. This mass resolution is closest to "level 3" in the AURIGA simulations.[54] This corresponds to approximately 6.4×10^6 particles in the stellar disk, 1.1×10^6 in the bulge, 1.2×10^6 in the gas disk, and 25.3×10^6 in the dark matter halo. We used a softening length of 0.02 kpc for all components.

Bar analysis

The analysis of various bar properties is performed as follows. First, the pattern speed is measured from the angle of the second Fourier component. We measured the second Fourier component by computing,

$$A_2 = \sum_i m_i e^{i2\phi_i}$$
$$A_0 = \sum_i m_i, \tag{2}$$

where m_i and ϕ_i are the mass and azimuthal angle of each particle, respectively. We computed A_2 and A_0 in cylindrical bins of width 0.5 kpc from radii of 0 to 30 kpc. We defined the angle of the bar ϕ_b to be twice the angle of the complex number A_2 as measured in the bin extending from a radius of 2.5 to 3 kpc. After correcting for the periodicity of ϕ_b, we measured the pattern speed as the two-sided finite gradient of ϕ_b as a function of time.

The time evolution of the bar strength, defined as the maximum of $|A_2/A_0|$ as a function of radius, is shown in Extended Data Fig. 3. The quantity $|A_2/A_0|$ varies from 0 to 1, with larger values indicating a stronger bar pattern. We see that in the N-body case, $|A_2/A_0|$ increases over time as the bar pattern slows. This is consistent with previous N-body simulations which showed a clear correlation between the bar pattern speed and the bar strength.[10] In the SMUGGLE case, we see that the bar strength has an initial drop but then remains at a roughly constant but slightly decreasing strength. This is consistent with the pattern speed in the SMUGGLE case being roughly constant or slightly increasing.

Computing the length of the bar and the torque on the bar by different components requires us to decompose the disk into a component which is trapped by the bar and a component which is untrapped. In order to do this, we follow closely the technique developed in ref.[55] We analyzed the orbit of each star particle (meaning initial disk, bulge, and newly formed stars) by extracting the x-y positions of the apoapse of each in a frame corotating with the bar (apoapses are defined as local maxima in r). For each apoapse, we searched for the 19 closest apoapses in time and applied a k-means clustering algorithm on this set of 20 points with $k = 2$. We then computed for each of the two clusters the average angle from the bar $\langle \Delta\phi \rangle_{0,1}$, the standard deviation in R of the points $\sigma_{R0,1}$, and the average radius of the cluster $\langle R \rangle_{0,1}$. At each apoapse, a particle was considered to be in the bar if it met the following criteria:

$$\max\left(\langle \Delta\phi \rangle_{0,1}\right) < \pi/8 \tag{3}$$

$$\frac{\sigma_{R0} + \sigma_{R1}}{\langle R \rangle_0 + \langle R \rangle_1} < 0.22 \tag{4}$$

These criterion are slightly different and simplified from the ones used in ref.[55], but we found to empirically work well at decomposing the disk into a bar and disk component. In Extended Data Fig. 4, we show an example of this decomposition. The *left* panel shows a surface density projection of the stellar disk and bulge (including newly formed stars) from the SMUGGLE model after 1 Gyr of evolution in a frame such that the bar is aligned with the x-axis. The *middle* panel shows a projection of the subset of stars that are identified as being trapped in the bar and the *right* panel shows a projection of the stars that are not identified as being trapped. The fact that the *right* panel is roughly axisymmetric indicates the bar decomposition is performing adequately.

After the disk has been decomposed into a trapped and untrapped component, we measured the bar length as being the radius R_b which encapsulates 99% of the stars identified as being trapped in the bar, allowing for some outliers. For the computation of the torque, we used the tree algorithm in `MakeNewDisk`[49] customized to be accessible from `Python` using `Cython`. This algorithm is based on the `TREESPH` code.[56] We constructed a tree using only the star particles identified as being trapped in the bar using an opening angle of 0.35. We then queried the tree at the locations of all resolution elements in the other components and computed the torque of the bar on such components. The torque on the bar by the other components is simply the negative of the torque on the other components by the bar. A similar method was applied in measuring the torque for the disk when the pattern speed is kept constant, as is done in Fig. 4.

Title

Next section.

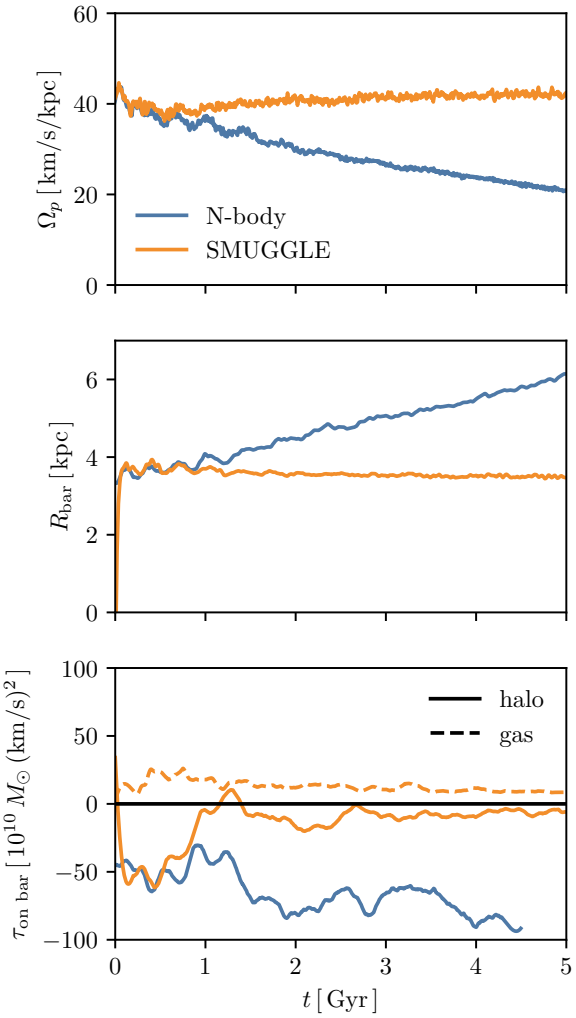

Figure 2: Various bar properties from the N-body and SMUGGLE runs. The *upper panel* show the evolution of the pattern speed. As expected, the bar in the N-body run slows down due to interactions between the bar and the dark matter halo. However, the bar in the SMUGGLE run does not slow down and instead remains at a constant pattern speed. The *middle panel* shows the evolution of the bar length. In the N-body case, the bar lengthens. This occurs because as the pattern speed drops, bar-like orbits at larger radii are possible. Stars are captured on these orbits, lengthening the bar. This process does not occur in the SMUGGLE cases since the bar pattern speed is not decreasing, and therefore the bar length remains constant. The *lower panel* shows the torque on the bar by different components. The solid lines show the torque exerted by the halo in both the N-body and SMUGGLE cases. The dashed line shows the torque exerted by the gas phase in the SMUGGLE run (there is no gas in the N-body run). Details on how these properties are calculated is given in the Methods section.

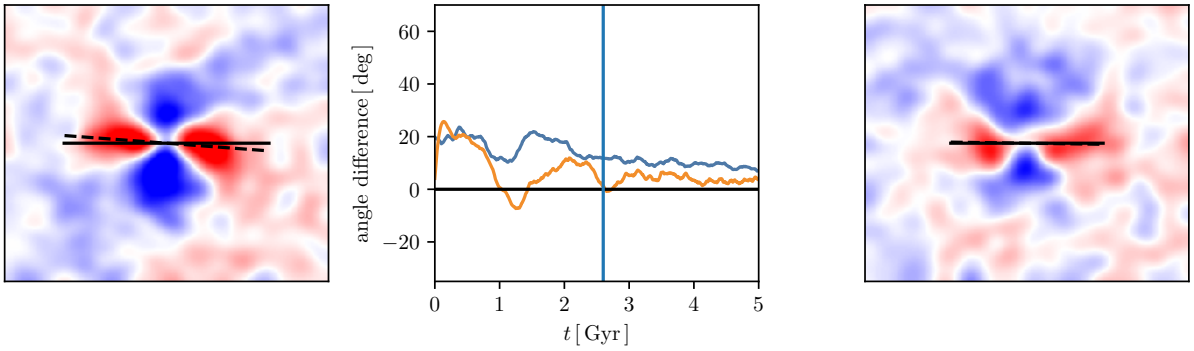

Figure 3: The wake excited in the dark matter halo in the N-body case (*left panel*) and SMUGGLE case (*right panel*) after 2.6 Gyr. The *left* and *right panels* show a surface density projection in the x-y plane of the dark matter halo after an axisymmetric average has been subracted. The solid line indicates the direction of the bar while the dashed line indicates the direction of the halo wake (both measured by taking the second Fourier component within a sphere of all material within a radius of X kpc). The *center panel* shows the time evolution of the angle difference between the bar and the halo wake, as measured from the second Fourier component. After the first Gyr, the angle difference in the SMUGGLE case is smaller than in the N-body case by about a factor of two, reflecting how the dark matter halo in the SMUGGLE case is unable to exert as negative a torque on the bar as in the N-body case.

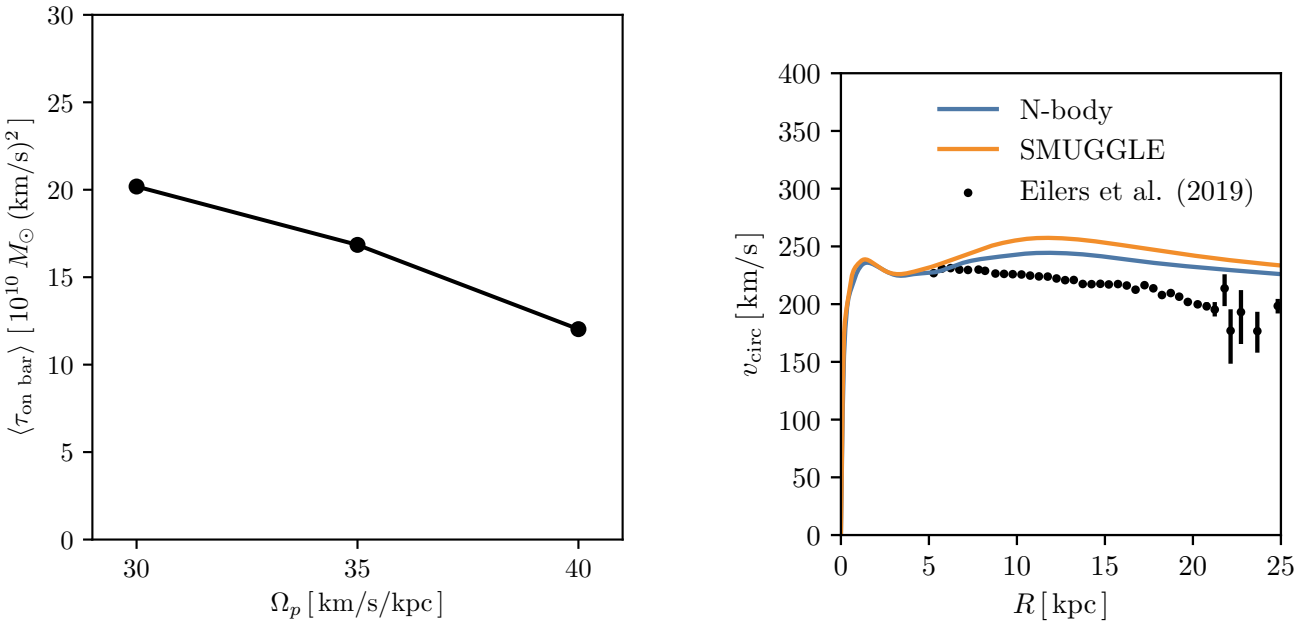

Figure 4: The torque on the bar by the gas when the pattern speed of the bar is kept at a constant value. Only gas within the corotation radius is able to infall. Since slower bars have larger corotation radii, slower bars experience a larger net torque than faster bars. The setup of the simulations used here is identical to the SMUGGLE case discussed earlier and in the Methods section, except the N-body disk is rotated as a solid body with a constant angular velocity.

The circular velocity curve for the N-body run (blue) and the SMUGGLE run (orange) compared to observational estimates.[52] We see that the circular velocity curve for both runs is marginally larger than the Milky Way's, but still comparable. The SMUGGLE circular velocity curve is larger than the N-body curve due to the additional mass in the gas phase.

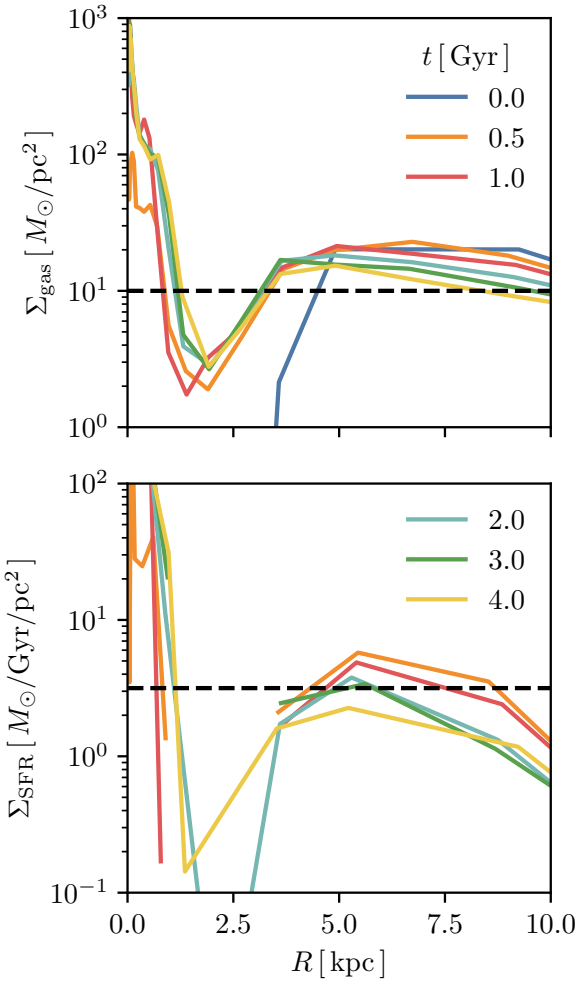

The time evolution of the gas surface density (*upper*) and the star formation rate (SFR) surface density (*lower*) at various times during the simulation. Colored lines indicate the profiles at selected times during the simulation while the horizontal dashed lines indicate approximate values for the Milky Way.[53] We see that the gas surface density is slightly higher but within an order of magnitude of the Milky Way's typical gas surface density. We see a sharp decrease in the gas and SFR surface density along the extent of the bar from $\sim$ 1 to $\sim$ 4 kpc, related to the gas inflow in this region. I will add the actual points from ref.[53] (Fig. 7), but just placing approx horizontal lines for now. The profiles are roughly flat anyways.

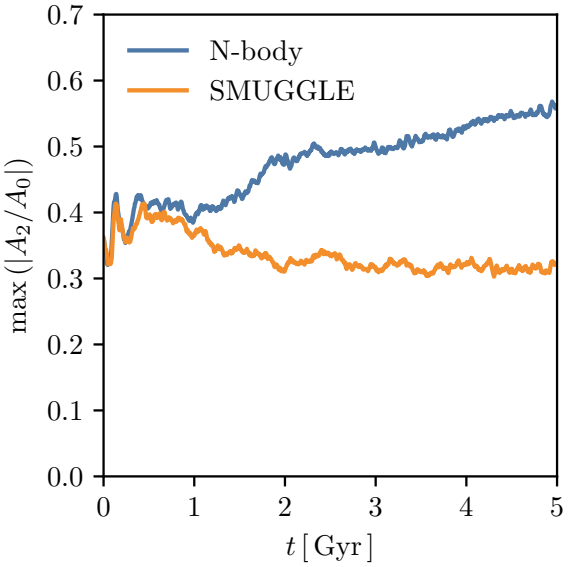

The time evolution of the bar strength, measured as the second Fourier component divided by the zeroth Fourier component (a formula is given in the Methods section). We see that in the N-body case (blue) the bar strength increases with time, consistent with previous results showing that the bar strength increases as bars slow down. In the SMUGGLE case (orange), we see that the bar strength remains roughly constant, possibly slightly decreasing with time. This is also consistent with the expected relation between pattern speed and strength since the bar in this case is not slowing down.

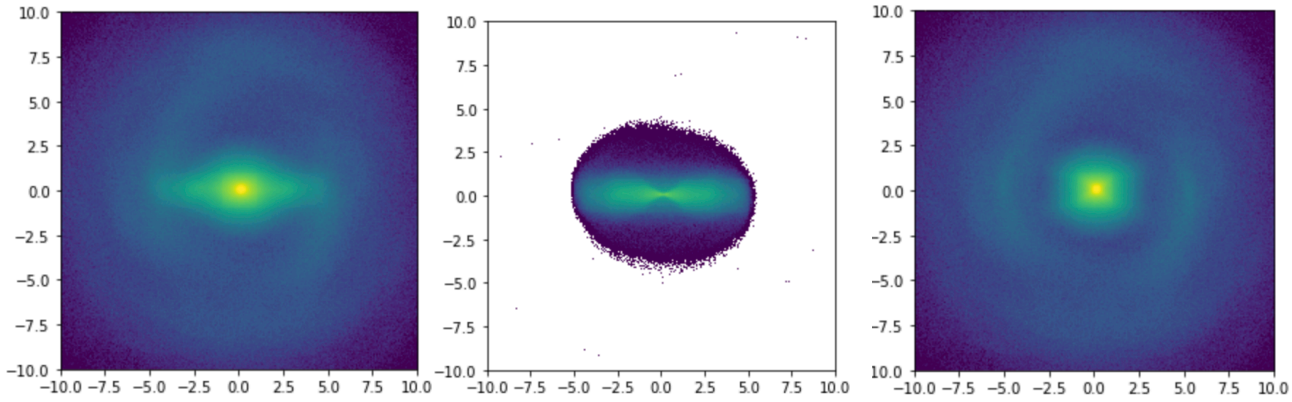

Demonstration of our bar decomposition procedure based on ref.[55] The *left panel* shows a surface density projection through the stellar component of the N-body simulation (disk and bulge). The *middle panel* shows the component of the disk identified as being trapped in the bar while the *right panel* shows the component of the disk identified as not being trapped in the bar. The fact that the untrapped stars form a roughly axisymmetric structure indicates our bar decomposition is sufficiently accurate. I will remake this figure - I ended up losing the files which stored the bar membership, so I just pulled these screenshots from an earlier presentation.